Title
Effects of Cd vacancies and unconventional spin dynamics in the Dirac semimetal Cd3As2

Journal
The Journal of Chemical Physics, 147(8)

ISSN
0021-9606

Authors
Koumoulis, Dimitrios
Taylor, Robert E
McCormick, Jeffrey
et al.

Publication Date
2017-08-28

DOI
10.1063/1.4999467

Peer reviewed

Effects of Cd vacancies and unconventional spin dynamics in the Dirac Semimetal Cd_3As_2

D. Koumoulis [1,5*], R. E. Taylor [1], J. McCormick [1], Y. N. Ertas [2], Lei Pan [3], Xiaoyu Che [3], Kang L. Wang [3], L-S. Bouchard [1,4*]

[1]*Department of Chemistry and Biochemistry, University of California Los Angeles, 607 Charles E. Young Drive East, Los Angeles, CA 90095, USA*

[2]*Department of Bioengineering, University of California Los Angeles, 420 Westwood Plaza, Los Angeles, CA 90095, USA*

[3]*Department of Electrical Engineering, University of California, Los Angeles, California 90095, USA*

[4]*California NanoSystems Institute, University of California Los Angeles, 570 Westwood Plaza, Los Angeles, CA 90095 USA*

[5]*Present address: School of Physical Science and Technology, ShanghaiTech University, Pudong, Shanghai 201210, China*

*Corresponding authors: Louis Bouchard and Dimitrios Koumoulis
Email address: louis.bouchard@gmail.com
dkoumoulis@shanghaitech.edu.cn

Cd_3As_2 is a Dirac semimetal that is a 3D analog of graphene. We investigated the local structure and nuclear-spin dynamics in Cd_3As_2 via ^{113}Cd NMR. The wideline spectrum of the static sample at 295 K is asymmetric and its features are well described by a two-site model with the shielding parameters extracted via Hertzfeld-Berger analysis

of the magic-angle spinning spectrum. Surprisingly, the ^{113}Cd spin-lattice relaxation time (T_1) is extremely long (T_1=95 s at 295 K), in stark contrast to conductors and the effects of native defects upon semiconductors; but it is similar to that of ^{13}C in graphene (T_1 = 110 s). The temperature dependence of $1/T_1$ revealed a complex bipartite mechanism that included a T^2 power-law behavior below 330 K and a thermally activated process above 330 K. In the high-temperature regime, the Arrhenius behavior is consistent with a field-dependent Cd atomic hopping relaxation process. At low temperatures, a T^2 behavior consistent with a spin-*1/2* Raman-like process provides evidence of a time-dependent spin-rotation magnetic field caused by angular oscillations of internuclear vectors due to lattice vibrations. The observed mechanism does not conform to the conventional two-band model of semimetals, but is instead closer to a mechanism observed in high-Z element ionic solids with large magnetorotation constant [Vega *et al., Phys. Rev. B* 74, 214420 (2006)].

Keywords: Vacancies, Hopping, Dirac semimetal, Graphene, Semiconductor, NMR

I. INTRODUCTION

Cadmium arsenide (Cd_3As_2) is a $A_3^{II}B_2^{V}$ chemically stable *n*-type semiconductor with high carrier mobility, which makes it a candidate for device applications[1-8]. Cd_3As_2 was predicted theoretically by Wang *et al.*[2] to be a Dirac semimetal (DSM). It has an inverted band symmetry mainly due to a strong spin-orbit coupling (SOC). Its 3D Dirac cones were recently observed experimentally[3]. Two dimensional (2D) or three dimensional (3D) Dirac semimetals include graphene and the 2D surface states of 3D topological insulators (TI) with

the Fermi level at the Dirac point inside the bulk band gap (Cd_3As_2, Na_3Bi etc.)[4]. Unconventional phenomena and physical properties including exotic electrical and thermal conductivity, high-temperature linear quantum magnetoresistance and oscillating quantum spin Hall effects have been detected by angle resolved photoemission spectroscopy (ARPES) and magneto-transport techniques[2-11].

Here, we have performed ^{113}Cd NMR measurements on Cd_3As_2. Due its ability to probe structural and band structure characteristics at specific atomic sites, nuclear magnetic resonance (NMR) spectroscopy can provide information that is hidden to other techniques (transport, ARPES etc.). In this study, NMR data in Cd_3As_2, accompanied by calorimetric and X-ray diffraction studies, are analyzed as function of temperature and magnetic field to shed light on the structural and electronic characteristics at a local level. A site inequivalence between the Cd atoms within the lattice was determined by static and magic angle spinning (MAS) spectral analysis. A two-site model with the shielding parameters extracted from the Hertzfeld-Berger analysis of the MAS spectrum describes the observed spectra. Interestingly, a bipartite spin-lattice relaxation mechanism was found to describe the entire relaxation process across the temperature (T) range. The power-law (T^2) dependence that occurs at the low-T regime is consistent with a nuclear spin-rotation relaxation mechanism, strongly effective in heavy Z-elements followed by a Cd hopping mechanism in the high-T regime, due to the large number of Cd vacancies that permit migration of Cd atoms within the lattice. The aforementioned complex relaxation process as a function of temperature and magnetic field bears resemblance to both the spin dynamics of ionic solids and graphene but is dissimilar to the one expected for conventional semimetals[41].

II. EXPERIMENTAL

The crystal structure of Cd_3As_2 was characterized at ambient temperature from powder samples using an X-ray diffractometer (XRD, Bruker D8 Discover Powder X-ray Diffractometer). Crystal structure analysis was performed at using Θ–2Θ scans, where the shape and width of the XRD spectra peaks were determined with the Rietveld refinement technique. Figure 1a shows the XRD patterns for the bare and annealed samples, which both reveal a polycrystalline sample. A diffraction peak analysis reveals the presence of tetragonal Cd_3As_2 (JCPDS: 21-0107) for both samples. The Rietveld refinement on the XRD pattern yields lattice constants of a = 12.6515 Å and c = 25.4432 Å. A second, hexagonal-close packed (hcp), Cd_2 phase (JCPDS: 00-8491) was also observed for both samples. The samples had hcp Cd_2 peaks for 2Θ = 31.78 and 38.45, which correspond to (002) and (011) crystal directions. Cd_3As_2 shows a tetragonal unit cell with the Cd atoms occupying tetrahedrally coordinated sites and As having cubic coordination. The crystal structure of Cd_3As_2 has been reexamined in consideration of the topological properties predicted for three-dimensional crystals[12]. The authors describe the crystal structure in terms of that of CaF_2, showing that the Cd is distributed in the cube-shaped array occupied by F in CaF_2, while the As is in the FCC positions occupied by Ca[12]. The crystal structure of Cd_3As_2 can be described relative to an anti-fluorite structure possessing 25% Cd site vacancy. The ordering or disordering of the vacancies affects the space group to which the crystal belongs[12].

Differential scanning calorimetry measurements on Cd_3As_2 were performed using a PerkinElmer DSC 8000 scanner across the temperature range T = 303–523 K at a rate of

5°C/min during upwards and downwards ramping. Figure 1b presents a series of small features from 334 to 355 K, including a sharp peak at 353 K (lower curve). These features are not observed upon temperature ramp-down (upper curve). This suggests that the sample undergoes an irreversible solid phase transition in this temperature regime. Around 225 ^{0}C (498 K) the system undergoes a phase transition from a primitive centrosymmetric tetragonal cell (space group P42/nmc) to a body centered tetragonal non-centrosymmetric unit cell (space group I41cd)[8,13,14]. Our temperature range of interest is below 400 K. The aforementioned structural phase transition is not probed by our NMR experiments. Additionally, a comprehensive chemical composition analysis was performed via Scanning Electron Microscopy and Energy Dispersive X-ray spectroscopy (SEM-EDS) in our sample (Figure 1c). The elemental mapping of the sample was performed using ZEISS Supra 40VP SEM at 25 kV. The *Kα* bands for Cd and As were outside the detectable range of the energy spectrum, where *Lα* bands were sufficient enough for detection and analysis. Cd and As peaks are clearly seen in the EDS spectra with weight percentages of 63% and 37%, respectively. The remaining small peaks which is mainly O (ambient oxygen) were not labeled for the sake of simplicity and purpose of this work. The percentage error in determining the weight content was less than 1%. These elemental mapping results indicate that the sample is composed of Cd and As. Lastly, our Cd_3As_2 sample is an *n*-type material. The carrier type of our sample was checked by a Hall coefficient measurement in a magnetic field of ±3 T at room temperature (Fig.1 inset).

The ^{113}Cd NMR data were acquired on a Bruker AV-600 spectrometer using both MAS and wideline techniques at a frequency of 133.20 MHz. Additional ^{113}Cd MAS and wideline data

were acquired on a Bruker DSX-300 spectrometer at 66.61 MHz. The ^{113}Cd chemical shift scale was calibrated using the unified Ξ scale[15], relative to the ^{113}Cd resonance of an aqueous solution of cadmium nitrate tetrahydrate. In particular, we have measured ^{113}Cd NMR spectra and spin-lattice relaxation rates ($1/T_1$) vs T.

III. RESULTS AND DISCUSSION

The ambient-temperature ^{113}Cd MAS spectrum of Cd_3As_2 spinning at 10 kHz is shown in Fig. 2. The spectrum consists of two isotropic peaks at -107 ppm and -356 ppm. The remaining peaks are spinning sidebands. A two-site Hertzfeld-Berger[16] model describes the spectral features. The shielding parameters of the model for the two sites extracted from the data are given in Table I. There are six different Cd sites in the structure[12,] with the "low temperature (LT) centrosymmetic $I4_1/acd$ structure", which corresponds to the temperature range for our NMR studies, having three unique Cd atoms[12]. Our MAS results resolve two main groups of resonance in a 2:1 ratio (4:2 site configuration). This suggests that two of the sites have virtually identical bonding environments.

It is interesting to note that the anisotropic shielding parameters obtained from the two-site model with the shielding parameters extracted from the Hertzfeld-Berger[16] analysis of the MAS spectrum reproduce the major features of the ^{113}Cd wideline spectrum of the static sample at 295 K, as shown in Fig. 3. The only spectral feature not reproduced is some spectral instensity around -238 ppm. This discrepancy in spectral intensity likely arises from the issue of exchange between the two sites. The explanation for the missing intensity of this peak in the simulation arises from the ^{113}Cd exchange between the two sites, which

yields a new resonance at the average of the two isotropic shifts (ca.-238 ppm) in the manner of a classic two-site exchange problem[18]. It should be noted that any additional resonance around -238 ppm in the MAS spectrum in Fig. 2 is obscured by the MAS spinning sidebands due to the residual width of the spinning sideband resonances, the proximity of the two isotropic resonances and their respective anisotropies. Varying the spinning speed did not readily reveal the existence of such a peak. The presence of such an additional resonance may be responsible for some of the uncertainty in the extracted shielding parameters from the MAS experiments. Rather than characterizing the dynamics of the exchange through spectral simulation, the nature of this exchange mechanism was analyzed with the nuclear spin-lattice relaxation data (*vide infra*).

All the resonances were temperature independent (220-380 K). Interestingly, the ^{113}Cd NMR results for the Dirac semimetal Cd_3As_2 stand in clear contrast to those usually found for conductors (metals) and also for nominally pure semiconductors in which native defects can produce significant charge carrier concentrations. This holds for both spectral shifts and spin-lattice ralaxation behavior. For example, the ^{113}Cd shifts in Cd_3As_2 are over 4,000 ppm away from the reported Knight shift of Cd metal[19], given as 4,324 ppm relative to an aqueous solution of cadmium nitrate[17]. The observed ^{113}Cd shift is in the range of diamagnetic materials. The differences in relaxation behavior are described below.

NMR relaxation measurements interrogate timescales associated with certain phonon or electron modes as well as a range of thermally activated processes. The ^{113}Cd spin-lattice relaxation times (T_1) at different temperatures were measured in saturation-recovery

experiments. The recovery curves were fitted by a single exponential function, $\frac{M_0 - M(t)}{M_0} = \exp\left(-\frac{t}{T_1}\right)$, where $M(t)$ represents the nuclear magnetization and M_0 is its value at thermal equilibrium. The extracted T_1 was extremely long, T_1=95 s, at ambient temperature (295 K). The ^{113}Cd spin-lattice relaxation rate for cadmium arsenide was also measured under MAS at ambient temperature. The two isotropic resonances under MAS at a spinning rate of 10 kHz were found to have the same ^{113}Cd T_1 value of 46 ± 2 s within experimental error at 295 K, in accordance with the observation of a single exponential saturation-recovery behavior from the static sample. Interestingly, these T_1 values are not descriptive of a metal or a semimetal[20]. However, similarly long T_1 times have been measured for graphene (110 s)[21]. Hence, in addition to the aforementioned observed ^{113}Cd shift, another remarkable difference with the expected semimetallic nature is the very long spin-lattice relaxation times.

Band structure calculations of Cd_3As_2 have determined that the electronic properties are mostly determined by the Cd-5*s* states (conduction band) and the As-4*p* states (valence band)[2]. From an NMR point of view, the interaction of *s*-state charge carriers in conductors and semiconductors results in a T_1 on the order of milliseconds or tens of milliseconds. As a specific example, the ^{207}Pb spin-lattice relaxation time in PbTe is 12 ms[20]. Therefore, based on the conventional Fermi liquid picture, the three orders of magnitude longer ^{113}Cd T_1 that was found here suggests little interaction with the charge carriers in spite of Cd_3As_2 being a semimetal. Moreover, the static sample has a T_1 of 59 s at 294 K at 7 T (and 95 s measured at 14 T). In short, the T_1 was also found to be magnetic-field dependent. At this point, it is

worth making a further comparison between the narrow-gap semiconductors like PbTe[20] or PbSe[22] and Cd_3As_2. In PbTe or PbSe, the native defects yield conduction electrons that shift the ^{207}Pb resonance from that of an insulator around 0 ppm to that of a semiconductor (mainly arising from native defects) with a resonance shift around 1,000 ppm, to finally obtain a Knight shift of metallic Pb at 1.47%[20,22]. In our case (^{113}Cd, Cd_3As_2), even with the high (25%) vacancy of Cd sites within the lattice (although these are not the native defects that give rise to conduction charge carriers), there is no indication of any nuclear shift resulting from interaction with the electrons at the Fermi surface. Nor is there any significant reduction in the relaxation rate, as was observed with Pb(Se,Te)[20,22], whose shift and number of carriers vary due to electronic inhomogeneity. Yet, the origin of the asymmetric resonances for Pb(Se,Te)[20,22] that were not narrowed under MAS due to the electronic inhomogeneity clearly differs from the asymmetic line in the static sample of ^{113}Cd of Cd_3As_2, which is easily narrowed by MAS, since it mainly results from shielding anisotropy effects.

A plot of ^{113}Cd $1/T_1$ vs T is shown in Fig. 4. The temperature dependence of $1/T_1$ of Cd_3As_2 in the low-T range follows a power-law[22], $\frac{1}{T_1} = A \cdot T^2$ (as a red straight line in Fig. 4) where $A = (1.18 \pm 0.05) \cdot 10^{-7}$ $s^{-1}K^{-2}$. This is evidence that low energy spin excitations at the ^{113}Cd NMR frequency are governed mainly by non-s character conduction electrons, counter to what is expected in conventional metals (Korringa law) and semi-metallic (two-band model) materials[23,41]. Previously, NMR studies from Young *et al.*[24], Koumoulis *et al.*[25] and Kobl *et al.*[26] have also observed a power-law behavior of $1/T_1T$ vs T in bulk topological insulators and GaAs epilayers. They have attributed it to the presence of native defects, disorder or a

high amount of vacancies within the lattice that can generate charge carriers and electronic inhomogeneity[42]. In the case of Cd_3As_2, the obtained T_1 (95 s) values are undoubtedly not representative of a metal or a semimetal. Thus, any interaction between the nuclear spins and the conduction carriers (hyperfine interaction) is most likely negligible and the Fermi-contact interaction does not provide a significant pathway for relaxation. As mentioned earlier, this is an unexpected result, considering that the band dispersion curves of Cd_3As_2[1,2] are mostly determined by the Cd-5*s* states (conduction bands). However, the present NMR results show that the Fermi-contact mechanism is not pertinent here. On the other hand, scalar relativistic effects and spin orbit effects in high-Z elements also have a strong impact on the electron-nucleus interactions and an effect on the NMR properties, since any change in the symmetry of the conduction bands (band inversion effect) also influences both the Cd nuclear magnetic shielding and the Cd spin dynamics and as a result the Fermi-contact term vanishes.

Recently, Okvatovity *et al.*[27] investigated the NMR dynamics in Weyl semimetals (WSM) theoretically. The WSM share quite parallel phenomenology to the Dirac semimetals. They have particularly investigated the hyperfine interaction between the Weyl fermions and the nuclear spins around the Weyl point[27]. In contrast to magnetic excitations around a parabolic ($E \propto k^2$) band dispersion (as expected in a conventional metallic material), the linear dispersion ($E \propto k$) leads to a strengthening of the orbital hyperfine contribution and the temperature-independent Korringa mechanism becomes a temperature-dependent process similar to the case of nodal superconductors (power-law temperature dependence)[39]. Specifically, in WSM the nuclear spin-lattice relaxation time closely behaves as in graphene

($T_1 \sim T^{-3}$) [27,40]. This nonlinear behavior is closer to the ^{113}Cd relaxation behavior but fundamentally different from that of a conventional metal or semimetal. Similarly, specific heat measurements in Cd_3As_2 revealed that the contribution of electrons even at low temperatures is negligible[28]. In addition, recent work by Zhang *et al.*[11] reported an unexpectedly low thermal conductivity of Cd_3As_2, smaller than that of a semiconductor or conventional (semi-) metal. Thus, the physical properties of Cd_3As_2 such as the electrical and thermal conductivity are different from those expected of semimetals, in line with our results.

In order to discuss more quantitatively the spin dynamics of Cd_3As_2 we take a closer look at the power-law temperature dependence of $1/T_1$ and compare it with other heavy-Z element materials. In particular, the T-dependence of $1/T_1$ reveals the observed power-law relaxation mechanism ($\frac{1}{T_1} = A \cdot T^2$) and the relaxation coefficient (A) is very close to that of α-SnF_2[29] [A = (2.21 ± 0.02)·10^{-7} s^{-1}K^{-2}], as well as of the same order of magnitude as Pb-containing compounds[30] *e.g.* $PbTiO_3$ [A = 9.00·10^{-7} s^{-1}K^{-2}]. The A coefficient (known also as the Raman constant) of Cd_3As_2 is almost identical to the one measured for α-SnF_2[29]. A is a measure of the spin-rotation coupling strength. Dividing A by the square of the gyromagnetic ratio (A/γ^2) gives an estimate of the role of the magnetic contributions ($\frac{1}{T_1} \propto \gamma^2$) to the lattice vibrations (phonons)[29,31]. In the case of Cd_3As_2, the calculated value ($10^{22} \cdot \frac{A}{\gamma^2}$), 0.37 s T^2K^{-2}, is close to the experimental result 0.22 s T^2K^{-2} for ^{119}Sn of α-SnF_2, but one order of magnitude smaller than the reported value for ^{207}Pb in $PbTiO_3$[29-32]. This suggests that the low-T relaxation pathway is driven by a Raman-*like* nuclear spin-rotation

relaxation mechanism[32] of ^{113}Cd nuclei in Cd_3As_2, akin to other heavy *Z*-elements that we have also previously reported, *e.g.* for ^{119}Sn and ^{125}Te nuclei as well as other lead-containing materials[29-32]. We conclude that the spin-rotation-*mediated* relaxation pathway in ^{113}Cd of Cd_3As_2 is similarly effective as the one for ^{119}Sn (α-SnF_2) but less effective than for ^{209}Pb ($PbTiO_3$). It should be noted that this relaxation mechanism is unrelated to the van Kranendonk[33] mechanism that is applicable in the case of quadrupolar nuclei (I >1/2). The Raman nuclear spin-rotation mechanism[32,34] encountered here is related to the modulation of the angular velocity[29] (instead of the angular momentum of a molecule in liquid phase) and its strength is proportional to the interatomic distance (nuclear spin-spin dipolar interaction)[29,32,34].

At high temperatures (T > 330 K) the NMR data follow a thermally activated mechanism (Arrhenius law), $\frac{1}{T_1} = B \cdot \exp\left(-\frac{E}{kT}\right)$. We found an activation energy of E=0.17 eV. The lower inset of Fig. 4 shows the Arrhenius plot of the high temperature data, shown as a red straight line (Fig. 4-inset). The calculated thermal activation energy obtained from the ^{113}Cd T_1 experiments as a function of temperature is consistent with the reported "hopping" of Cd vacancies in similar types of materials[35,36] and supports the theoretical study by Plenkiewicz *et al.*[37]. As described by Conte *et al.*[38], the two Cd vacancies are diagonally opposite each other in one face of a small cube. This may explain the existence of the two observed sites in the ^{113}Cd spectrum. The ^{113}Cd lineshape of Cd_3As_2 does not shift or change noticeably over this temperature range. The observed migration of the Cd vacancies provides an explanation of the site exchange mechanism. In addition, the hopping mechanism is magnetic-field-dependent as the difference in Hz between the two resolved shifts depends linearly on the

magnetic field, as seen here. The validity of the aforementioned relaxation mechanism is further supported by the observed magnetic field dependence of T_1 as at 300 MHz (95 s at 295 K) and 600 MHz (59 s at 294 K). All the above results confirm that Cd vacancies have a strong impact on the physical properties and band structure characteristics of Cd_3As_2. Finally, the overall temperature dependence of the spin-lattice relaxation process (Fig. 4) can now be described via a bipartite mechanism as $\frac{1}{T_1} = A \cdot T^2 + B \cdot \exp\left(-\frac{E}{kT}\right)$, with A = $(1.18 \pm 0.05)\cdot 10^{-7}$ $s^{-1}K^{-2}$ and E=0.17 eV as the activation energy for the high temperature activation process.

IV. CONCLUSIONS

In summary, we have carried out ^{113}Cd NMR experiments in the Dirac semimetal Cd_3As_2. The ^{113}Cd spectra are asymmetric due to a site inequivalence between the cadmium atoms within the lattice. The MAS results resolve two main groups of resonance in a 2:1 ratio. We observe a crossover from a power-law behavior (T^2) of the spin-lattice relaxation rate ($1/T_1$) at lower temperatures to Cd site hopping dynamics at high temperatures. Surprisingly, the observed magnitude of the observed T_1 values, the magnitude and sign of the ^{113}Cd resonance shifts, the magnetic field dependence of $1/T_1$ of Cd_3As_2 are in direct contradiction to those typically found for conductors, semiconductors and semimetals, in spite of its semimetallic band structure. Its electronic properties are closer to graphene than a typical semimetal.

TABLES & FIGURES

TABLE I. ^{113}Cd Shielding Tensor Parameters of Cd_3As_2

Experiment	δ_{11}	δ_{22}	δ_{33}	δ_{iso}	ζ_{csa}[c]	η[d]	Ω[e]	κ[f]

Site 1 10 kHz MAS[a,b]	+110	-116	-325	-105	-220	0.97	437	+0.03
Site 2 10 kHz MAS[a,b]	-208	-412	-480	-355	+159	0.43	272	-0.5

[a]Chemical shifts referenced to neat dimethylcadmium by use of 0.5 M $Cd(NO_3)_2$ in H_2O as a secondary reference assigned as -49 ppm[17].
[b]Estimated uncertainties in the principal components of the shielding tensor as measured by MAS are ±15 ppm.
[c]$\zeta_{csa} = \delta_{33} - \delta_{iso}$.
[d]$\eta = (\delta_{22} - \delta_{11})/\zeta_{csa}$.
[e]$\Omega = |\delta_{33} - \delta_{11}|$.
[f]$\kappa = 3(\delta_{22} - \delta_{iso})/\Omega$.

FIGURES CAPTIONS

FIG. 1. (Color online) The X-ray diffraction patterns for the bare (red) and annealed (black) Cd_3As_2 which both reveal a polycrystalline nature (a). Differential scanning calorimetry measurements on Cd_3As_2, measuring from 303–523 K at 5 °C/min during temperature ramping upwards and downwards (b) and the Hall coefficient measurement at 300 K in a magnetic field of ±3 Tesla (b-inset). Chemical composition analysis via Scanning Electron Microscopy and Energy Dispersive X-ray spectroscopy (c).

FIG. 2. (Color online) ^{113}Cd MAS spectrum at 295 K. The experimental spectrum is in blue with a two-site simulation along with the summation (shown by the red dotted curve).

FIG. 3. (Color online) ^{113}Cd wideline spectrum at 295 K. The experimental spectrum is in blue. The simulated spectrum (red curve) consists of a two-site model. The shielding parameters are listed in Table I.

FIG. 4. (Color online) The nuclear spin-lattice relaxation rate ($1/T_1$) in Cd_3As_2 as a function of temperature. The low-T data are consistent with a spin-*1/2* Raman mechanism ($A \cdot T^2$) via nuclear spin-rotation interaction (upper left inset). Above 330 K the data follow a

thermally activated mechanism [$B \cdot \exp\left(-\frac{E}{kT}\right)$] with an energy scale (0.17 eV) associated with the cadmium hopping process (lower right inset).

ACKNOWLEDGMENTS

We acknowledge the use of instruments at the Molecular Instrumentation (MIC) facility at UCLA, which included funding from the MRI program of the National Science Foundation under grant no.1532232.

References

[1]B. Dowgaiallo-Plenkiewicz and P. Plenkiewicz, "Symmetry properties of the energy bands of Cd_3As_2 type crystals," Phys. Stat. Sol. (B) **94**, K57-K60 (1979).

[2]Z.J. Wang, H.M. Weng, Q.S. Wu, X. Dai, Z. Fang, "Three-dimensional Dirac semimetal and quantum transport in Cd_3As_2," Phys. Rev. B **88**, 125427 (2013).

[3]Z.K. Liu, J. Jiang, B. Zhou, Z.J. Wang, Y. Zhang, H.M. Weng, D. Prabhakaran, S.K. Mo, H. Peng, P. Dudin, T. Kim, M. Hoesch, Z. Fang, X. Dai, Z.X. Shen, D.L. Feng, Z. Hussain, Y.L. Chen, "A stable three-dimensional topological Dirac semimetal Cd_3As_2," Nat. Mater. **13**, 677–681 (2014).

[4]Z.K. Liu, B. Zhou, Y. Zhang, Z.J. Wang, H.M. Weng, D. Prabhakaran, S.K. Mo, Z.X. Shen, Z. Fang, X. Dai, Z. Hussain, Y.L. Chen, "Discovery of a Three-Dimensional Topological Dirac Semimetal, Na_3Bi," Science **343**, 864 (2014).

[5]M. Neupane, S.Y. Xu, R. Sankar, N. Alidoust, G. Bian, C. Liu, I. Belopolski, T.R. Chang, H.T. Jeng, H. Lin, A. Bansil, F. Chou, M.Z. Hasan, "Observation of a three-dimensional topological Dirac semimetal phase in high-mobility Cd_3As_2," Nat. Commun. **5**, 3786 (2014).

[6]Y. Feng, Z. Wang, C. Chen, Y. Shi, Z. Xie, H. Yi, A. Liang, S. He, J. He, Y. Peng, X. Liu, Y. Liu, L. Zhao, G. Liu, X. Dong, J. Zhang, C. Chen, Z. Xu, X. Dai, Z. Fang, X.J. Zhou, "Evidence of Topological Surface State in Three-Dimensional Dirac Semimetal Cd_3As_2," Sci. Rep. **4**, 5385 (2014).

[7]R. Sankar, M. Neupane, S.-Y. Xu, C. J. Butler, I. Zeljkovic, I.P. Muthuselvam, F.-T. Huang, S.-T. Guo, S.K. Karna, M.-W. Chu, W. L. Lee, M.-T. Lin, R. Jayavel, V. Madhavan, M.Z. Hasan & F. C. Chou, "Large single crystal growth, transport property, and spectroscopic characterizations of three-dimensional Dirac semimetal Cd_3As_2," Sci. Rep. **5**, 12966 (2015).

[8]S. Borisenko, Q. Gibson, D. Evtushinsky, V. Zabolotnyy, B. Büchner, and R. Cava, "Experimental Realization of a Three-Dimensional Dirac Semimetal," Phys. Rev. Lett. **113**, 027603 (2014).

[9]T. Liang, Q. Gibson, M.N. Ali, M. Liu, R. J. Cava, and N.P. Ong, "Ultrahigh mobility and giant magnetoresistance in the Dirac semimetal Cd_3As_2," Nat. Mater. **14**, 280-284 (2015).

[10]C.X. Liu, H. Zhang, B. Yan, X.L. Qi, T. Frauenheim, X. Dai, Z. Fang, S.C. Zhang, "Oscillatory crossover from two-dimensional to three-dimensional topological insulators," Phys. Rev. B **81**, 041307(R) (2010).

[11]C. Zhang, T. Zhou, S. Liang, J. Cao, X. Yuan, Y. Liu, Y. Shen, Q. Wang, J. Zhao, Z. Yang, "Unexpected low thermal conductivity and large power factor in Dirac semimetal Cd_3As_2," Chinese Phys. B **25**, 017202 (2015).

[12]M.N. Ali, Q. Gibson, S. Jeon, B.B. Zhou, A. Yazdani, R.J. Cava, "The Crystal and Electronic Structures of Cd_3As_2, the Three-Dimensional Electronic Analogue of Graphene," Inorg. Chem. **53**, 4062–4067 (2014).

[13]H. Okamoto, "The As-Cd (arsenic-cadmium) system," J. Phase Equilibria **13**, 147 (1992).

[14]A. Pietraszko, K. Lukaszewicz, "Thermal expansion and phase transitions of Cd_3As_2 and Zn_3As_2," Phys. Stat. Sol. (A) **18**, 723 (1973).

[15]R.K. Harris, E.D. Becker, S.M.C. de Menezes, R. Goodfellow, P. Granger, "NMR nomenclature. Nuclear spin properties and conventions for chemical shifts (IUPAC Recommendations 2001)," Pure Appl. Chem. **73**, 1795 – 1818 (2001).

[16]J. Herzfeld, A.E. Berger, "Sideband intensities in NMR spectra of samples spinning at the magic angle," J. Chem. Phys. **73**, 6021-6030 (1980).

[17]D.R. Franke, H. Eckert, "Structural studies of covalent nonoxidic glasses: solid state cadmium-113 wide-line, magic angle-spinning, and spin-echo NMR spectroscopy of glasses in the system cadmium arsenide ($CdAs_2$)-cadmium germanium arsenide ($CdGeAs_2$)," J. Phys. Chem. **95**, 331-336 (1991) .

[18]J.A. Pople, W. G. Schneider, H. J. Bernstein, *High Resolution Nuclear Magnetic Resonance* (McGraw-Hill Book Company, New York, 1959), pp. 218.

[19]E.R. Andrew, W.S. Hinshaw, R.S. Tiffen, "NMR in rapidly rotated metallic aluminium and cadmium," J. Magn. Reson. **15**, 191-195 (1974).

[20]R. Taylor, F. Alkan, D. Koumoulis, M.P. Lake, D. King, C. Dybowski, L-S. Bouchard, "A Combined NMR and DFT Study of Narrow Gap Semiconductors: The Case of PbTe," J. Phys. Chem. C **117**, 8959–8967 (2013).

[21]A.M. Panich and G.B. Furman, "Nuclear spin–lattice relaxation and paramagnetic defects in carbon nanomaterials," Diam. Relat. Mater. **23**, 157-161 (2012).

[22]D. Koumoulis, R.E. Taylor, D. King, Jr., L.-S. Bouchard, "NMR study of native defects in PbSe," Phys. Rev. B **90**, 125201 (2014).

[23]N. Bloembergen, "Nuclear magnetic relaxation in semiconductors," Physica **20**, 1130 (1954).

[24]B.-L. Young, Z.-Y. Lai, Z. Xu, A. Yang, G.D. Gu, Z.-H. Pan, T. Valla, G.J. Shu, R. Sankar, and F.C. Chou, "Probing the bulk electronic states of Bi_2Se_3 using nuclear magnetic resonance," Phys. Rev. B **86**, 075137 (2012).

[25]D. Koumoulis, B. Leung, T.C. Chasapis, R.E. Taylor, D. King Jr, M.G. Kanatzidis, L.-S. Bouchard, "Understanding Bulk Defects in Topological Insulators from Nuclear-Spin Interactions," Adv. Func. Mater. **24**, 1519-1528 (2014).

[26]D. Kölbl, D. M. Zumbühl, A. Fuhrer, G. Salis, and S.F. Alvarado, "Breakdown of the Korringa law of nuclear spin relaxation in metallic GaAs", Phys. Rev. Lett. **109**, 086601 (2012).

[27]Z. Okvátovity, F. Simon, and B. Dóra, "Anomalous hyperfine coupling and nuclear magnetic relaxation in Weyl semimetals," Phys. Rev. B **94**, 245141 (2016).

[28]K. Bartkowski, G. Pompe, E. Hegenbarth, "Specific heat of single crystalline Cd_3As_2, Cd_3P_2 and Zn_3P_2 at low temperatures," Phys. Stat. Sol. (A) **111**, K165 (1989) .

[29]G. Neue, S. Bai, R. E. Taylor, P. A. Beckmann, A.J. Vega, C. Dybowski, "^{119}Sn spin-lattice relaxation in α-SnF_2," Phys. Rev. B **79**, 214302 (2009).

[30]L.-S. Bouchard, A.O. Sushkov, D. Budker, J.J. Ford, A.S. Lipton, "Nuclear-spin relaxation of ^{207}Pb in ferroelectric powders," Phys. Rev. A **77**, 022102 (2008).

[31]A.J. Vega, P.A. Beckmann, S. Bai, C. Dybowski, "Spin-lattice relaxation of heavy spin-1/2 nuclei in diamagnetic solids: A Raman process mediated by spin-rotation interaction," Phys. Rev. B **74**, 214420 (2006).

[32]P.A. Beckmann, S. Bai, A.J. Vega, and C. Dybowski, "^{207}Pb spin-lattice relaxation in solid $PbMoO_4$ and $PbCl_2$," Phys. Rev. B **74**, 214421 (2006).

[33]J. van Kranendonk, "Theory of quadrupolar nuclear spin-lattice relaxation," Physica **20**, 781 (1954).

[34]J.B. Grutzner, K. W. Stewart, R. E. Wasylishen, M. D. Lumsden, C. Dybowski, P.A. Beckmann, "A New Mechanism for Spin−Lattice Relaxation of Heavy Nuclei in the Solid State: ^{207}Pb Relaxation in Lead Nitrate," J. Am. Chem. Soc. **123**, 7094–7100 (2001).

[35]R.D. Gould and B.B. Ismail, "Observations of Low Temperature Hopping Conduction in Evaporated Cadmium Telluride Thin Films Using Current–Temperature Measurements," Phys. Stat. Sol. (A) **134**, K65-K68 (1992).

[36]Q. Li, H. Li, H. Fan, W. Jie, M. Xu, H. Wang, "Electrical conduction behavior and hopping rates estimate of cadmium zinc telluride single crystal," J. Cryst. Growth **372**, 175-179 (2013).

[37]B. Plenkiewicz, P.R. Wallace, P. Plenkiewicz, "The role of vacancies in the band structure of Cd_3As_2," Solid State Commun. **50**, 681-684 (1984).

[38]A. M. Conte, O. Pulci and F. Bechstedt, "Electronic and optical properties of topological semimetal Cd_3As_2," Sci. Rep. **7**, 45500 (2017).

[39]K. Asayama, Y. Kitaoka, G.-Q. Zheng, K. Ishida, Y. Tokunaga, "NMR study of strongly correlated superconductors (heavy fermions, high T_c and related materials)", *Studies of High Temperature Superconductors*, *Advances in Research and Applications* Vol. 29 (Nova Science Publishers, Inc., New York, 1999), pp. 60.

[40]B. Dora, F. Simon, "Hyperfine interaction in graphene: The relevance for spintronics", Phys. Status Solidi (b) **247**, 2935 (2010).

[41]D. Koumoulis, J.P. Scheifers, R. Touzani, B.P.T. Fokwa, L.S. Bouchard, "Pseudogap formation and vacancy ordering in the new perovskite boride Zr_2Ir_6B", Acta Materialia **120**, 32-39 (2016).

[42]D. Koumoulis, T. Chasapis, B. Leung, R.E. Taylor, C.C. Stoumpos, N.P. Calta, M.G. Kanatzidis, L.S. Bouchard, "Site-specific contributions to the band inversion in a topological crystalline insulator", Adv. Electr. Mater. **1**, 1500117 (2015).

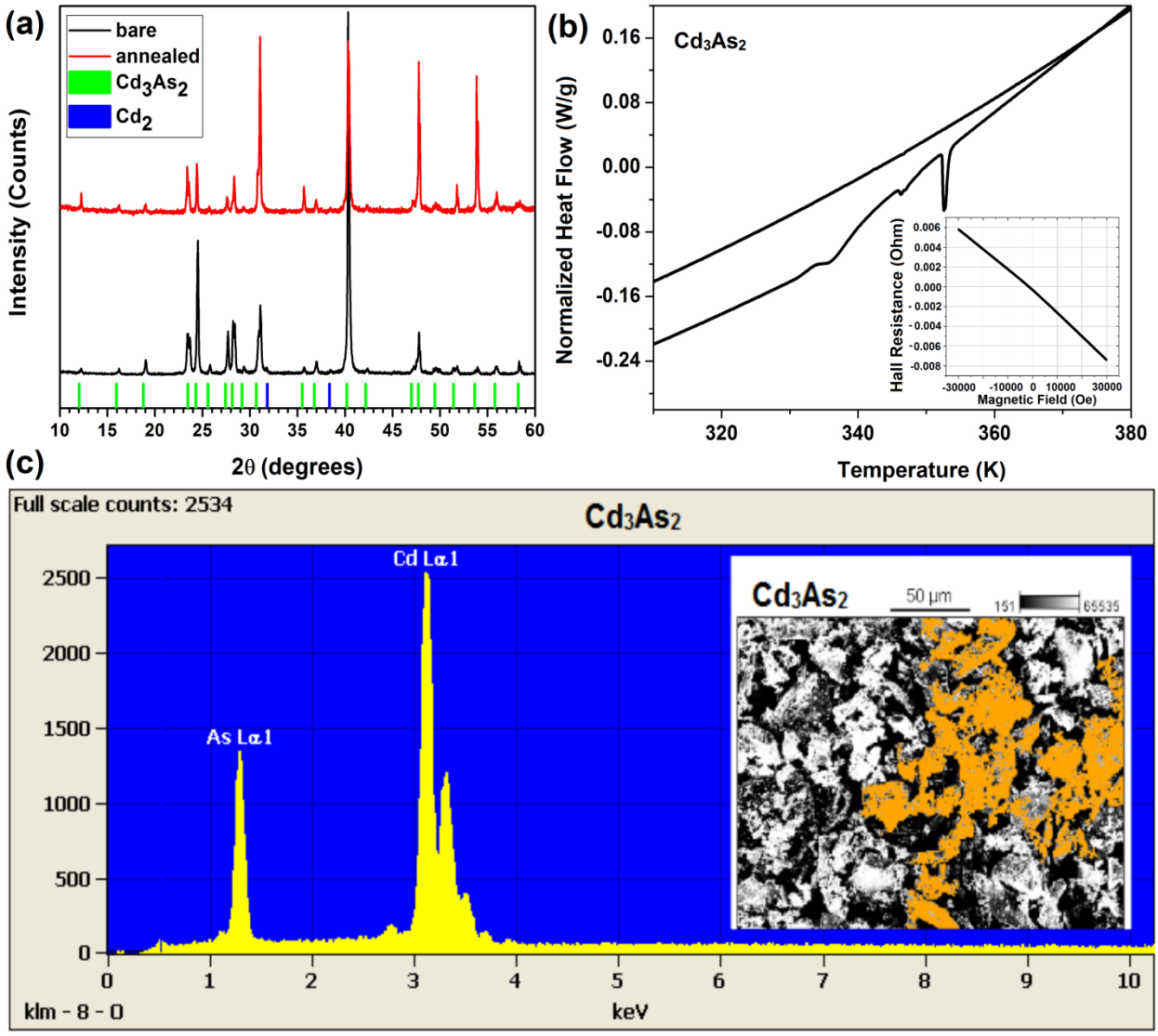
(a)
bare
annealed
Cd3As2
Cd2
Intensity (Counts)
2θ (degrees)
(b)
Cd3As2
Normalized Heat Flow (W/g)
Temperature (K)
Hall Resistance (Ohm)
Magnetic Field (Oe)
(c)
Full scale counts: 2534
Cd3As2
Cd Lα1
As Lα1
Cd3As2
50 µm
151
65535
klm - 8 - 0
keV

FIG. 1.

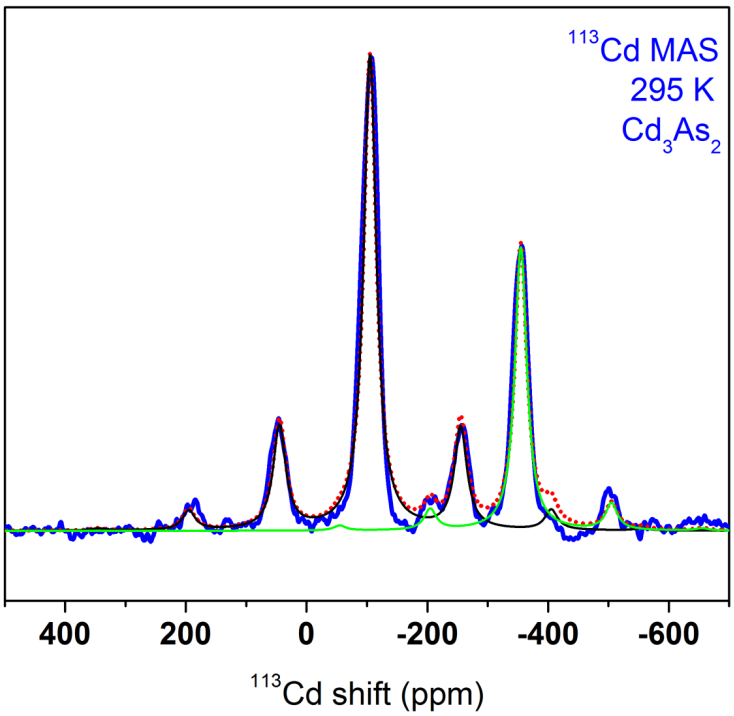

FIG. 2.

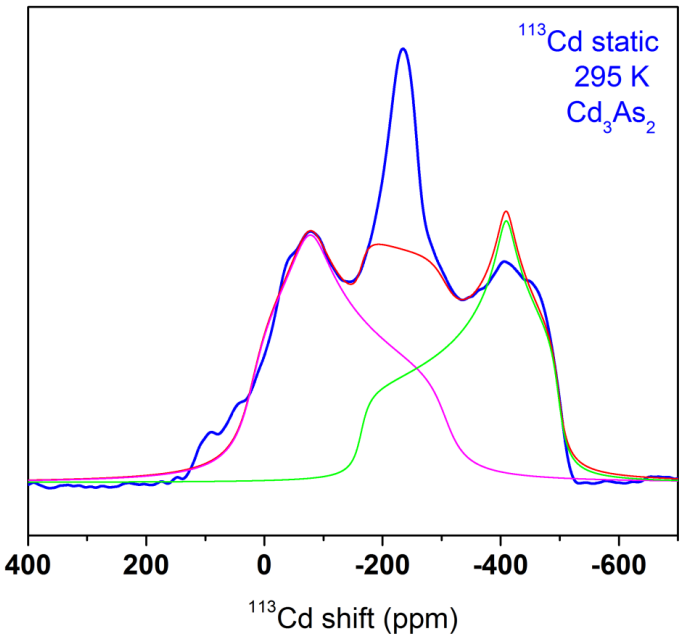
^{113}Cd static
295 K
Cd_3As_2
400
200
0
-200
-400
-600
^{113}Cd shift (ppm)

FIG. 3.

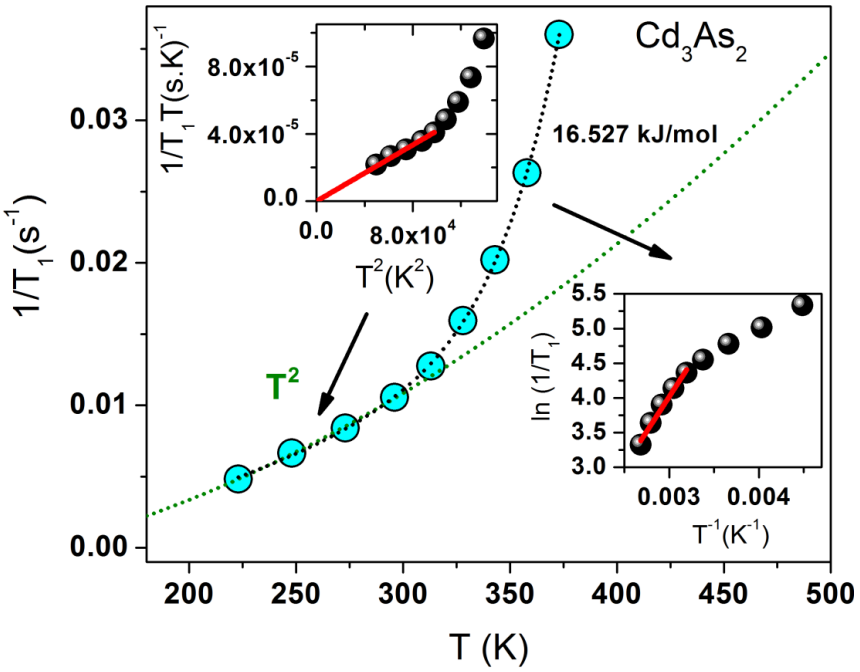

FIG. 4.